Different mechanisms of cluster explosion within a unified smooth particle hydrodynamics Thomas-Fermi approach: Optical and short-wavelength regimes compared

Marian Rusek and Arkadiusz Orłowski
Institute of Physics, Polish Academy of Sciences, Aleja Lotników 32/46, 02-668 Warsaw, Poland
(Received 20 October 2004; published 14 April 2005)

The dynamics of small ($\leqslant$55 atoms) argon clusters ionized by an intense femtosecond laser pulse is studied using a time-dependent Thomas-Fermi model. The resulting Bloch-like hydrodynamic equations are solved numerically using the smooth particle hydrodynamics method without the necessity of grid simulations. As follows from recent experiments, absorption of radiation and subsequent ionization of clusters observed in the short-wavelength laser frequency regime (98 nm) differs considerably from that in the optical spectral range (800 nm). Our theoretical approach provides a unified framework for treating these very different frequency regimes and allows for a deeper understanding of the underlying cluster explosion mechanisms. The results of our analysis following from extensive numerical simulations presented in this paper are compared both with experimental findings and with predictions of other theoretical models.

DOI: 10.1103/PhysRevA.71.043202 PACS number(s): 36.40.Gk, 32.80.−t, 52.50.Jm

I. INTRODUCTION

Clusters are aggregates of atoms containing up to a few thousands atoms. Usually they are formed in expanding high-pressure gas jets. Atomic clusters have properties intermediate between those of an isolated atom and the bulk or solid-state material. The study of the interaction of such species with electromagnetic radiation is an increasingly active research field. Clusters are as easily penetrated by a laser beam as gaseous media and, at the same time, exhibit a large absorption of laser energy comparable to that of solid targets [1].

Laser interaction with atomic clusters differs substantially from that of simple atomic and molecular systems. Experiments on clusters irradiated by intense laser pulses in the optical regime have revealed efficient generation of extremely highly charged atomic ions [2–8] and production of highly energetic particles (both electrons and ions), with kinetic energies of the MeV order [6,7,9–11].

Several theoretical models have been proposed to explain the mechanism underlying the production of highly charged energetic ions in interaction of atomic clusters with intense laser pulses with frequencies in the optical range. In classical Monte Carlo simulations of cluster explosion the nuclei and unbound electrons are treated as classical particles obeying Newton's equations of motion [12–16]. The bound electrons are released with a certain probability depending on the electric field strength inside the cluster [12–15] and on collisions with other electrons and ions [13,14].

Recently an application of the time-dependent density functional theory to a study of the response of atomic clusters to an intense laser pulse appeared [17]. A simplified one-dimensional model with frozen ion positions and correlation effects neglected allowed numerical solution of the time-dependent Kohn-Sham equations describing electron dynamics in a cluster. Results concerning the initial stage of ionization in the moderate intensity regime were presented.

Intense short-wavelength radiation opens many new research areas in physics and chemistry. The photon energies in the vacuum ultraviolet (vuv) frequency range are large enough for the single photons to ionize irradiated matter. Since the binding energies of the electrons characterize individual elements, the ability to ionize matter allows direct insight into electronic structure and chemical composition of materials. On the other hand, the wavelength in the vuv regime is comparable to the atom spacing in solids, and, therefore, the diffraction of short-wavelength radiation allows one to determine the geometric structure of complex elements with atomic resolution.

Until now experiments were hindered by the lack of sufficiently intense short-wavelength light sources. This situation is presently changing. Free-electron lasers making use of linear accelerators are expected to combine the advantages of synchrotron radiation (short wavelength) with those of lasers (intense short pulses) and thus to pave the way to new types of experiments. Recently, the study of the interaction of intense vuv free-electron laser pulses with xenon [18] and argon [19] clusters has been reported.

It can be expected that the strong-field—matter interaction in the short-wavelength vuv regime is considerably different from that at optical frequencies. The ponderomotive energy (average kinetic energy of a free electron oscillating in the radiation field) is a parameter that characterizes to some extent the interaction. For a typical optical pulse it reaches the values of several hundred eV whereas in the case of a short-wavelength pulse used in the DESY experiments [18,19] it has a value of hundreds of meV. Therefore field ionization, which is a dominant process in the optical domain, can hardly account for observations in the short-wavelength realm. Thus additional ionization and subsequent explosion mechanisms should be considered in the case of rare-gas-atom clusters exposed to short-wavelength radiation [18].

At first glance the well-understood physics that describes the laser pulse energy absorption by the cluster in the optical domain seems not to work in the frequency range used in the DESY experiments [18]. A standard inverse bremsstrahlung model applied to the absorption of short-wavelength radia-

tion by xenon clusters [18] predicted an absorption of only a few photons per atom. This differs from the experimentally measured value by more than an order of magnitude.

It turned out that the problem was in the choice of the ionic scattering potential [20]. It seems that in a dense plasma formed by illuminating a xenon cluster with a vuv pulse the electrons experience more than just a Coulomb potential. By using a Yukawa-like form of the screening potential the authors of [20] have shown that their implementation of the inverse bremsstrahlung model is able to reproduce the large number of vuv photons observed in the experiment [18].

A similar situation occurs in the case of the argon clusters irradiated by a short-wavelength laser pulse. In a recent experiment [19] each argon atom in the cluster absorbed on average up to 20 photons while losing two electrons. Also in this case the standard collisional heating model cannot fully account for the strong laser energy absorption.

In this paper we further extend and refine a time-dependent Thomas-Fermi model introduced in our previous paper [21] to describe the dynamics of argon clusters in an intense laser pulse. Both optical *and* short-wavelength regimes are analyzed and the explosion mechanisms are compared. A simplified one-dimensional version of a similar model has been already successfully applied to the description of cluster explosion in the optical frequency regime [22,23]. In our previous work a three-dimensional model produced promising results for argon atoms and six atom argon clusters subjected to an optical pulse [21]. A slightly refined version of the model allowed us to extend these previous results to a more realistic case of a 55-atom cluster in three dimensions [24]. The current version of the model permits us also to attack the short-wavelength case (for preliminary numerical evidence see [25]). In the present paper we go much further by analyzing the realistic case of larger clusters, providing a synthetic physical interpretation encompassing both cases. The results obtained in the present paper look very promising and seem to agree with the experimental findings [19].

Note that the time-dependent Thomas-Fermi model used automatically yields a Yukawa-type screening of the Coulomb potential used in [20]. This was shown in our previous paper [21] in the case of a simplified relation of the internal energy of the electron gas (ρ^2 instead of $\rho^{5/3}$). Our theoretical treatment does not require the assumption of thermodynamical limit used in [20] and thus does not limit us to the study of "sufficiently large" clusters. Also the perturbation theory is no longer needed, which allows us in principle to go to the higher intensities where nonlinear effects may arise.

The Bloch-like hydrodynamic equations resulting from the time-dependent Thomas-Fermi model are solved numerically using the smooth particle hydrodynamics (SPH) method. This attractive (although still a bit controversial [26]) method of solving partial differential equations was, so far, popular only in astrophysics. Since its introduction by Lucy [27] and Gingold and Monaghan [28] this method has become a standard technique for modeling a variety of astrophysical problems. Examples are the collapse and fragmentation of gas clouds [29–33], interstellar cloud collisions [34,35], protostar formation [36,37], the stability of stars [38], binary star collisions [39], and galaxy formation [40]. Our paper seems to be one of the first attempts to use the SPH method to solve problems from a different field of physics, namely, to model the ionization of atomic clusters. Successful application of the SPH method in this case is nontrivial as it requires dealing with the singularity of the Coulomb potential close to the nuclei of the cluster atoms.

This paper is organized as follows. In Sec. II the time-dependent Thomas-Fermi model is introduced. Then in Sec. III the details of the smooth particle hydrodynamics numerical calculations are presented. In Sec. IV we check the results coming from the model in the optical frequencies regime. The main results concerning short-wavelength pulses are described in Sec. V. Finally we finish with a brief summary.

II. THEORETICAL MODEL

The Thomas-Fermi model introduced in the mid 1920s by Thomas [41] and independently by Fermi [42] embodies many of the features of the modern density functional methods [43,44]. Within this model the ground-state structure of an atomic cluster is described by the average electron density $\rho(\vec{r})$ and the positions of the nuclei $\vec{R}_a$. It can be obtained by minimization of the following Thomas-Fermi energy functional $\mathcal{E}_{\mathrm{TF}}$ which is a sum of the internal and potential energies [21]:

$$\mathcal{E}_{\mathrm{TF}} = \mathcal{E}_{\mathrm{int}} + \mathcal{E}_{\mathrm{pot}}. \tag{1}$$

In the equation above the relations for the internal (kinetic) energy $\mathcal{E}_{\mathrm{int}}$ of an ideal electron gas at temperature $T=0$ are used locally:

$$\mathcal{E}_{\mathrm{int}} = c_k \int d^3r[\rho(\vec{r})]^{5/3}, \quad c_k = \frac{3}{5}\frac{\hbar^2}{2m}[3\pi^2]^{2/3}, \tag{2}$$

and the potential energy $\mathcal{E}_{\mathrm{int}}$ of mutual Coulomb interactions of electrons and nuclei is given by

$$\mathcal{E}_{\mathrm{pot}} = \frac{e}{2}\int d^3r\left[\sum_{a=1}^{N} Z\delta(\vec{r}-\vec{R}_a) - \rho(\vec{r})\right]\Phi(\vec{r}), \tag{3}$$

where the self-consistent Coulomb potential $\Phi(\vec{r})$ reads as

$$\Phi(\vec{r}) = e\int \frac{d^3r'}{|\vec{r}-\vec{r}'|}\left[\sum_{a=1}^{N} Z\delta(\vec{r}'-\vec{R}_a) - \rho(\vec{r}')\right]. \tag{4}$$

Here N is the number of atoms in the cluster, e is the elementary charge, and m denotes the electron mass.

The collective Thomas-Fermi model is most valid for heavy atoms, with many electrons. It has been used for the calculation of ionization potentials of different atomic numbers and ionization degrees [45]. In this paper we use the time-dependent version of the Thomas-Fermi model to describe ionization of argon atoms (atomic number $Z=18$). Even for such a relatively low value of Z the ionization potentials calculated in [45] agree well with real values in some range of ionization degree (at low ionization degree the method breaks down because of the lack of exchange, while

for high degree only a few electrons remain and the statistical Thomas-Fermi approach stops working). This is confirmed in [46] where multiphoton ionization of noble-gas atoms in strong laser fields is explained theoretically using the Thomas-Fermi model. The results compare favorably with experiments.

To introduce a time-dependent version of the Thomas-Fermi model we assume that the electron density at any point of space is obtained by summing up the contributions from n smoothed pseudoparticles [21]:

$$\rho(\vec{r}) = \frac{ZN}{n}\sum_{j=1}^{n} f_j(\vec{r} - \vec{r}_j) \tag{5}$$

[the functions f_j are assumed to be normalized, $\int d^3r\, f_j(\vec{r}) = 1$].

The dynamics of the electron density (5) and the motion of the nuclei are governed by the following Hamiltonian in which the Thomas-Fermi energy functional (1) plays the role of the potential energy term [21]:

$$\mathcal{E} = \mathcal{E}_{\mathrm{kin}} + \mathcal{E}_{\mathrm{TF}}, \tag{6}$$

and the kinetic energy (of translational motion) of electrons and nuclei reads as

$$\mathcal{E}_{\mathrm{kin}} = \sum_{a=1}^{N} \frac{M\vec{V}_a^2}{2} + \int d^3r \rho(\vec{r}) \frac{m[\vec{v}(\vec{r})]^2}{2} \tag{7}$$

(M denotes the nuclear mass).

After inserting Eq. (5) into Eq. (6) and assuming that the functions f_j are sufficiently δ-like (i.e., neglecting terms of the second order in the characteristic widths of the kernel functions f_j [47,48]) one arrives at the following Hamilton equations of motion for the smoothed pseudoparticle positions $\vec{r}_j$ (cf. [21]):

$$m\frac{d^2\vec{r}_i}{dt^2} = -\frac{2}{3}\sum_{j=1}^{n}\left(\frac{c_k}{\rho_i^{1/3}} + \frac{c_k}{\rho_j^{1/3}}\right)\vec{\nabla}_i w_{ij}(\vec{r}_i - \vec{r}_j) + e\vec{\nabla}_i\Phi_i \tag{8}$$

where

$$w_{ij}(\vec{r}) = \frac{ZN}{n}\int d^3r' f_i(\vec{r}' - \vec{r}) f_j(\vec{r}') \tag{9}$$

and the transition between field quantities $F(\vec{r})$ ($F = \rho, \vec{v}, \Phi, \ldots$) and pseudoparticle-based quantities F_i is done in the following way:

$$F_i = \int d^3r f_i(\vec{r} - \vec{r}_i) F(\vec{r}). \tag{10}$$

Equations (8) can be understood as a discretized smooth particle hydrodynamics [27,28] version of the Bloch-like hydrodynamic equations [49]. Therefore, by treating the Thomas-Fermi energy functional as the potential energy part of the Hamiltonian of the system we viewed the oscillations of the electron cloud in an atomic cluster as the motion of a fluid characterized by a density $\rho(\vec{r},t)$ and a velocity field $\vec{v}(\vec{r},t)$. A similar hydrodynamic model has been used in the weak-field limit to study photoabsorption of an atom in free space [50] and in plasma [51]. Also multiple ionization of xenon atoms by a strong laser field was studied using a two-dimensional version of a similar model [52].

The hydrodynamic equations for the electron density ρ are supplemented by the Newton-like equations of motion for the positions of the nuclei $\vec{R}_a$:

$$M\frac{d^2\vec{R}_a}{dt^2} = -Ze\vec{\nabla}\Phi(\vec{R}_a). \tag{11}$$

The interaction with the laser pulse is treated within the dipole approximation by replacing the electrostatic Coulomb potential in Eq. (4) by

$$\Phi(\vec{r}) \to \Phi(\vec{r}) - \vec{r}\cdot\vec{\mathcal{F}}, \tag{12}$$

where $\vec{\mathcal{F}}$ is the electric field of the incoming wave. The linearly polarized wave of a pulse used in the simulations is assumed to have a field envelope proportional to sine squared with a full width at half maximum τ and an optical period τ_0:

$$\vec{\mathcal{F}}(t) = \vec{\mathcal{F}}_0 \sin^2\left(\frac{\pi}{2\tau}t\right)\cos\left(\frac{2\pi}{\tau_0}t\right). \tag{13}$$

Note that the theoretical approach presented here includes several possible ionization mechanisms: above-the-barrier (or field) ionization both by an external laser field and by an internal field due to the space-charge distribution inside the cluster, as well as (to some extent) electron-impact (or collisional) ionization.

III. CALCULATION DETAILS

The electron density in a neutral Thomas-Fermi atom is singular at the nucleus. At large distances from the nucleus r it falls off as r^{-6} rather than exponentially [53]. An electron cloud of an ion has a finite cutoff radius. In order to model the electron density of Thomas-Fermi atoms and ions as a sum of smoothed pseudoparticles (5) one should in principle use a variable pseudoparticle width: narrower pseudoparticles to model the electron cloud in the vicinity of the nucleus, and wider pseudoparticles to model the outer shells of the atom (or ion).

In our previous paper [21] we utilized f_j from Eq. (5) in the form of a Gaussian function *identical* for all pseudoparticles:

$$f(\vec{r}) = \left(\frac{\alpha}{\sqrt{\pi}}\right)^3 e^{-(\alpha\vec{r})^2}. \tag{14}$$

It turned out, however, that this choice of fixed width of all pseudoparticles leads to some problems in modeling the electron cloud close to the nucleus. Several pseudoparticles were stacking on top of each other and the smooth particle hydrodynamic method used was breaking down. To prevent this we have chosen a large value of the parameter α ($\alpha = 7$ for $Z = 18$ and $n/N = 125$) from Eq. (14). That choice increased the maximum force appearing in the simulations, which in turn made the numerical code extremely slow and

caused any realistic calculations to be nearly impossible.

Let us stress that the condition of validity of the Thomas-Fermi theory is not well obeyed near nuclei where the singular Coulomb potential varies rapidly over a characteristic electron wavelength. Therefore instead of modeling the electron cloud close to the nucleus with a large number of test particles of very small width we made a more physical choice—the electron density of an atom is modeled by test particles of two kinds: one large particle originally centered at the nucleus which represents the core electrons and a large number of smaller particles modeling the outer shells of the atom:

$$\rho(\vec{r}) = \frac{ZN}{n}\left\{ \xi\left[\sum_{j=1}^{n} f(\vec{r}-\vec{r}_j)\right] + (1-\xi)\frac{n}{N} g(\vec{r}-\vec{r}_0)\right\}, \tag{15}$$

where f is given by Eq. (14) and

$$g(\vec{r}) = \left(\frac{\beta}{\sqrt{\pi}}\right)^3 e^{-(\beta\vec{r})^2}. \tag{16}$$

We have chosen $\beta = 1/r_0$ where r_0 is the radius of the Thomas-Fermi ion of charge $Z(1-\xi)$ (i.e., $Z\xi$ electrons remain to be bound) [54]:

$$r_0 = 3.173\,61\frac{\sqrt{(1-\xi)/\xi}}{Z^{1/3}}. \tag{17}$$

The parameter α from Eq. (14) was chosen to model well an isolated Thomas-Fermi atom of given Z [21]. For this value of α the Thomas-Fermi energy relations are preserved [53]:

$$2\mathcal{E}_{\text{int}} + \mathcal{E}_{\text{pot}} = 0. \tag{18}$$

This choice was done in the following way. First the ground states of an atom corresponding to several different values of α were prepared. It turns out that the relation (18) holds only for a certain value of α, which was than used to model the interaction of the cluster with the laser pulse. For example for $n/N = 125$ pseudoparticles per atom (this is the value used later in the paper) and $Z = 18$ (argon atoms) we have found $\alpha = 5$ for $\xi = 0.1$ and $\alpha = 1.5$ for $\xi = 0.5$.

Let us mention that because the collective Thomas-Fermi model is basically statistical in nature, it cannot be applied directly to the low-electron-density regions, as in the outer shells of the neutral atom. By modeling the electron density of an atom by a *finite* number of pseudoparticles we in fact introduce some cutoff radius and these low-density regions are not considered. By changing the parameter ξ from Eq. (15) we can manipulate the value of this cutoff and chose how well the outer shells of an atom should be modeled. For example, in the case of $\xi = 0.1$ (and $\alpha = 5$) the cutoff radius is small, and therefore the outer shells are not well modeled. In the second case of $\xi = 0.5$ (and $\alpha = 1.5$) the cutoff radius is larger, and therefore the outer shells are modeled better (at the expense of the core electrons which in this case are represented by a single Gaussian function).

Ground-state properties of small clusters of rare-gas atoms have been investigated extensively in the literature (see, e.g., [55–58]). The usual theoretical approach is to describe the atoms in a cluster as a system of particles interacting via a short-range potential such as, e.g., the Lennard-Jones potential. It has been reported that particularly stable configurations of such clusters are of the form of a closed-shell icosahedron. For example, an $N = 55$-atom cluster consists of two icosahedral shells and one atom in the middle; the second shell can be separated into two subshells with different radii.

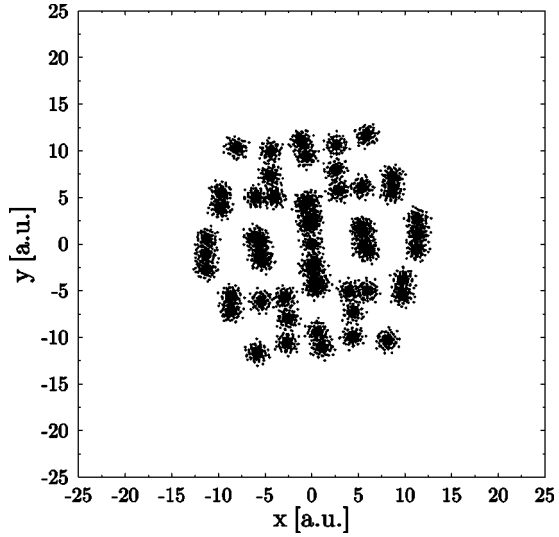

FIG. 1. Ground-state structure of an $N = 55$-atom cluster with $\xi = 0.1$. Equilibrium positions of the nuclei $\{\vec{R}_a\}$ are marked by filled circles. Small black dots correspond to the positions of the pseudoparticles modeling the equilibrium electronic density ρ.

We downloaded from [59] the publicly available ground-state structures of $N = 55$-atom Lennard-Jones clusters and used them as the equilibrium positions of the nuclei in the Thomas-Fermi model. The positions of the nuclei were rescaled so that equilibrium distance between two atoms is $R_0 \simeq 7$ a.u. $= 3.7$ Å which is similar to the spacing of atoms in argon clusters [60]. Next they were used as input into the hydrodynamic calculations involving the motion of an electron fluid. The resulting example ground-state structures are shown in Figs. 1 and 2. Let us note that in Fig. 1 the electron clouds of individual atoms are well separated. On the contrary, in Fig. 2 we observe the larger radius of the pseudoparticles as compared to Fig. 1. This allows us to model the electron cloud in between the atoms with greater accuracy.

Notice that, as shown by [61], additional corrections are needed to the Thomas-Fermi functional in order to model interatomic bonds. However, it turned out that in the case of a cluster illuminated by a short 100 fs pulse considered in this paper, the ground-state structure of a cluster obtained by a minimization of the standard Thomas-Fermi functional turned out to be stable enough during the time of interest.

In the next step we make use of the two obtained ground states to proceed with the simulations. We are concerned with the interaction of the laser pulses with these clusters.

IV. INFRARED PULSE

Let us first check how well our model works in the optical frequency domain. The ground-state cluster structure from

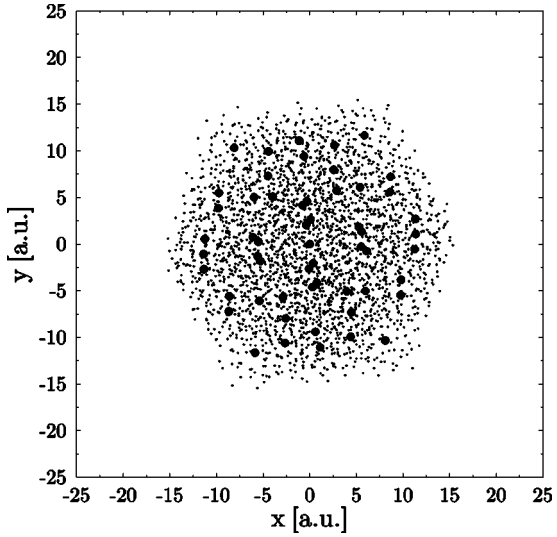

FIG. 2. Ground-state structure of an $N=55$-atom cluster with $\xi=0.5$. Equilibrium positions of the nuclei $\{\vec{R}_a\}$ are marked by filled circles. Small black dots correspond to the positions of the pseudoparticles modeling the equilibrium electronic density ρ.

Fig. 1 will now be illuminated by a typical laser pulse of infrared frequency (a similar pulse was used, e.g., in the experiments in [62]). The atoms of the cluster have initially no kinetic energy and are subject to an oscillating electric laser field at intensity $I=1.4\times10^{15}$ W/cm^2 (or $\mathcal{F}_0=0.2$ a.u.). The pulse used in the simulations had a wavelength $\lambda=800$ nm and a temporal full width at half maximum $\tau=106.67$ fs (or $\tau/\tau_0=40$). The electric field of the pulse was polarized linearly along the x axis. The same pulse parameters were used in our previous paper [21] (where only a six-atom cluster was studied).

In Fig. 3 we plot the internal (2), potential (3), kinetic (7), and total energy of a 55-atom argon cluster illuminated by a laser pulse versus time. It is seen that the Thomas-Fermi energy relations are preserved at the initial time, i.e., the

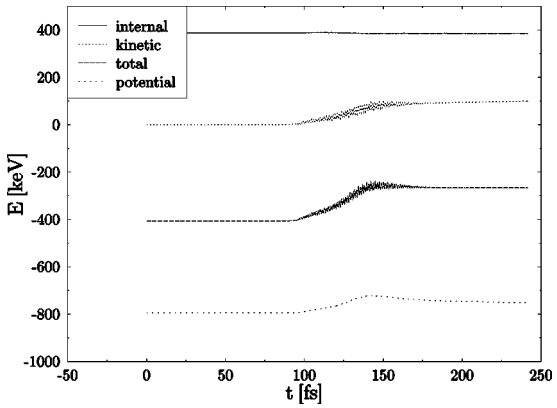

FIG. 3. Potential, kinetic, internal, and total energy of a 55-atom argon cluster illuminated by a laser pulse plotted versus time. The Thomas-Fermi energy relations are preserved at the initial time. Total energy absorbed from the laser pulse is clearly visible. Efficient laser energy absorption starts when the pulse envelope approaches its maximal value.

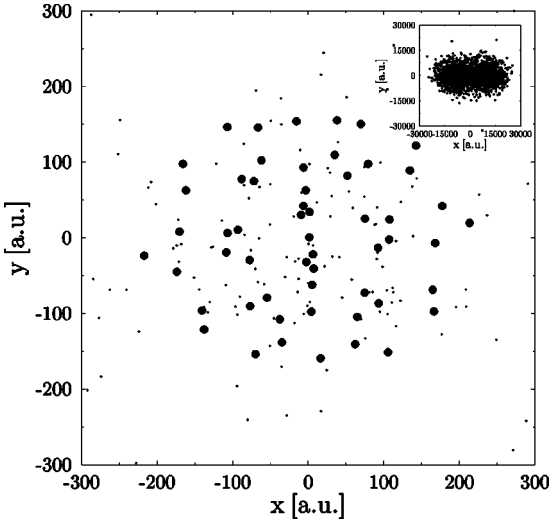

FIG. 4. Excited $N=55$-atom cluster from Fig. 1 at the end of the laser pulse at $t=250$ fs. Positions of the nuclei $\{\vec{R}_a\}$ are marked by filled circles. Small black dots correspond to the positions of the pseudoparticles modeling the electronic density ρ. The inset shows the electron cloud at a 1:100 magnification (i.e., the x and y coordinates vary from −3000 to 3000 a.u.).

potential energy is twice as large as the internal energy with a minus sign as in Eq. (18). At later times the electric field of the laser becomes strong enough to start above the barrier ionization of the cluster atoms (tunnel ionization, which may happen at lower values of the field, is not described by our semiclassical model). Thus inner ionization starts. The electrons released from the individual atoms still remain bound by the cluster as a whole. Next they are ejected from the cluster by the still increasing pulse (outer ionization) and start to oscillate in the electric field of the laser. As seen from inspection of Fig. 3 this happens at $\simeq$80 fs: at this time the oscillations of the total kinetic energy become visible. These laser-driven electrons are effectively heated through collisions with the cluster ions (inverse bremsstrahlung). It follows from Fig. 3 that such an efficient laser energy absorption starts when the pulse envelope approaches its maximal value. This absorbed energy is then converted into translational energy of the ions and the cluster disintegrates by a Coulomb explosion process. At the end of the pulse the kinetic energy of the ions grows at the expense of the potential energy and the total energy remains constant. Thus the total energy absorbed from the laser pulse is clearly visible.

In Fig. 4 we present the structure of the cluster just after the pulse is finished. The size of the cluster is more than ten times larger than the ground-state structure from Fig. 1. The inset shows the electron cloud at a 1:100 magnification (i.e., the x and y coordinates vary from −30 000 to 30 000 a.u.). It is seen that the electrons are ejected mainly along the pulse polarization axis (i.e., along the x axis).

It follows from inspection of Fig. 4 that almost all free electrons were removed from the cluster by the laser pulse. This observation makes the calculation of the charges of the outgoing ions feasible. They were calculated in the following way. For each pseudoparticle its charge is added to the charge of the closest ion; pseudoparticles that are further

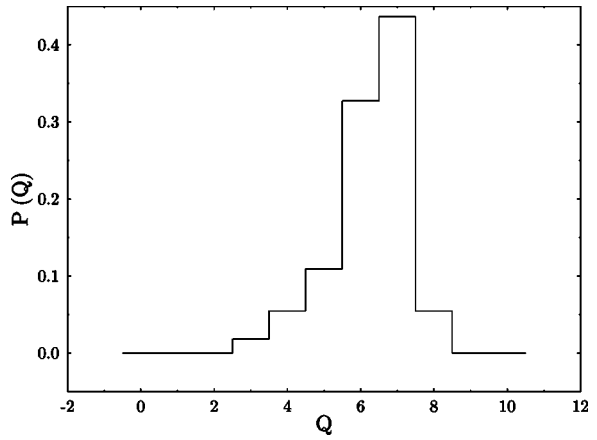

FIG. 5. Distribution of the final charges of the ions formed in the explosion of a 55-atom cluster. They agree with both experimental results and recent theoretical predictions.

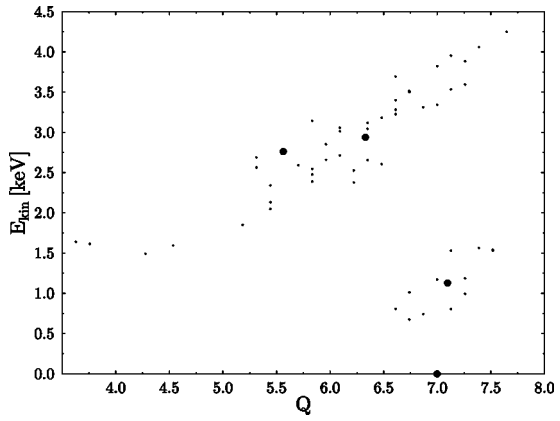

FIG. 6. Kinetic energy of the ions plotted as a function of the charge state. Small dots correspond to individual ions while larger filled circles represent results averaged over (sub)shells. The linear dependence of the ion energy on ion charge seems to be a good approximation for each (sub)shell.

from any ion than 10 a.u. are considered lost. In Fig. 5 we plot the resulting distribution of the final charges of the ions formed in the explosion of the cluster. Charges as high as +8 are observed. The results are consistent with both experimental results by Purnell *et al.* [62] and theoretical predictions by Ishikawa and Blenski [12]. It is seen from inspection of Fig. 5 that it is not possible to tell from which shell of the cluster an ion is coming just by looking at its charge. What we need is both charge *and* kinetic energy.

Thus in Fig. 6 we have the kinetic energy of the ions plotted as a function of the charge state. Small dots correspond to individual ions while larger filled circles represent results averaged over (sub)shells. The linear dependence of the ion energy on ion charge seems to be a good approximation for each (sub)shell. For argon clusters Coulomb repulsion is the key explosion mechanism [8]. Thus ion energy should have a quadratic dependence on ion charge [1,7]. As shown theoretically by Ishikawa and Blenski [12] (who also observed linear dependence for given shells) it is possible to get the experimentally observed quadratic dependence by summing contributions from different cluster shells and/or different laser intensity regions.

Note that the ions coming from the outer shells of the cluster (leaving the cluster first) are more energetic than those coming from the inner shells (leaving the cluster later). Such a stepwise character of the explosion has been suggested as an explanation of phenomena observed in experiments [8] and confirmed within one-dimensional (1D) numerical simulations using a similar time-dependent Thomas-Fermi hydrodynamic model [22] as well as with our previous simulations [21].

Therefore from Fig. 6 we conclude that the most ionized atoms come from the inner shells of the cluster. This shows the dependence of atomic ionization rates on the original position of an atom in the cluster and is in agreement with results of a 1D time-dependent density functional theory simulations [17]. Let us present the following explanation of this observation. Field ionization induced by an external laser field starts at the same time for all atoms of the cluster. Next the ionization of the inner shell seems to be slowed down by the presence of the outer shells of the cluster. At later times the outer shells explode and ionization of the inner shell is strongly enhanced by electron-impact ionization due to the laser-field-driven oscillations of the electrons liberated from the cluster atoms. Since these electrons oscillate mainly along the linear polarization axis of the laser pulse, they do not affect the outer shells of the cluster, which are already far away from the original position of the cluster.

One of the main motivations behind the laser-cluster interaction studies was probably the desire to generate photons with energies much larger than the energy of a single laser photon. One of the possible high-energy-photon generation mechanisms is high-order-harmonic generation in strong laser fields. Note that due to the nonlinearity inherent in the Thomas-Fermi model it is also possible to see some traces of this effect in our simulations. We have calculated the dipole moment d of the cluster from Fig. 1 illuminated by an infrared laser pulse. Its squared Fourier transform is plotted in Fig. 7 as a function of the frequency. We see that odd harmonics of the incoming wave are generated during the clus-

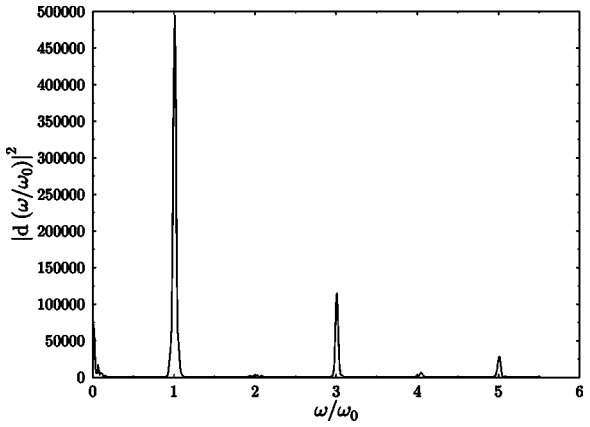

FIG. 7. Radiation spectrum of the cluster plotted as a function of the frequency relative to the frequency of the laser pulse. Odd harmonics are generated during the cluster explosion process. The spectrum falls off for the first harmonics (later a plateau is expected).

ter explosion process (the generation of even harmonics requires particular spatial symmetry of the nonlinear medium). This will be contrasted with the short-wavelength case.

Let us mention, that we have also tried to explode the second ground-state structure from Fig. 2 using the same infrared laser pulse. However, in this case the results we got are unphysical. Indeed, in the case of $\xi=0.5$ as many as nine core electrons are modeled by a single Gaussian particle. For a high ionization degrees (cf. Fig. 5) this leads to wrong results: at the end of the pulse each atom was ionized only four times. Thus the dynamics of the core electrons seems to play an important role in the cluster explosion at optical frequencies.

V. ULTRAVIOLET PULSE

Encouraged by reasonable results coming from the time-dependent Thomas-Fermi model in the optical frequencies regime we would like now to apply it to the description of DESY experiments with argon clusters [19]. In these experiments small ($\leqslant$900 atoms) argon clusters were illuminated by focused free-electron laser radiation at a power density up to 10^{14} W/cm^2. At such a high power density the absorption and ionization of argon clusters with vuv radiation turn out to be independent of the wavelength and the specific electronic structure of the cluster [19]. Thus the semiclassical Thomas-Fermi model seems to be a reasonable choice in this intensity regime.

At 98 nm laser wavelength the energy of a single photon is 12.7 eV. Since the ionization potential of Ar atoms is 15.5 eV, at least two photons were needed to ionize each atom. The laser energy absorption in a cluster is strongly enhanced. In a cluster each Ar atom absorbs up to 20 photons and loses on average two electrons.

Let us first illuminate by a short-wavelength pulse of ultraviolet frequency the 55-atom argon cluster ground state from Fig. 1. The pulse used in the simulations had a wavelength 98 nm (or $\tau_0=13.527$ a.u.), temporal full width at half maximum of 50 fs (or $\tau/\tau_0=150$), and peak intensity of 10^{14} W/cm^2 (or $|\vec{\mathcal{F}}_0|=0.05$ a.u.). It turns out that in this case there is practically no laser energy absorption. The clusters survive the pulse intact and no atoms get ionized.

We conclude that the vibrations of the core electrons that were well modeled in the optical case are not relevant. They eventually could start playing a role at higher vuv pulse intensity, as suggested in [63], where a simple man's (one-dimensional) model was used. We proved, however, that in the intensity regime considered in this paper, an even more sophisticated 3D not-that-simple man's model does not help in explaining the strong energy absorption observed in experiments.

One possible source of this problem may be the fact that the Thomas-Fermi model works well only in a certain ionization degree regime. Indeed the authors of [45] studied ionization potentials of different atoms using the Thomas-Fermi model. In the case of $Z=20$ (a Z number close to 18 for argon) and ionization degrees of the order of 0.1 (close to the experimental result) the ionization potential coming from the model is overestimated by factor of 3.

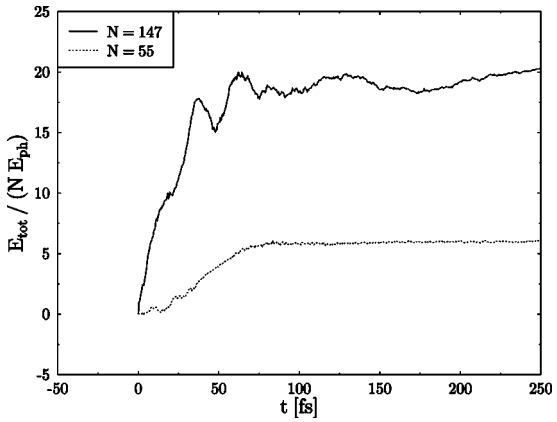

FIG. 8. Total energy absorbed by clusters of different sizes subjected to short-wavelength laser pulse plotted as a function of time. The results are presented in average number of photons absorbed per atom. The energy acquired by the cluster increases strongly with its size.

Another possible reason for the discrepancy between theoretical and experimental results is a poor modeling of the outer shells of the Thomas-Fermi atoms within our numerical method. This assertion is supported by Fig. 1 where the cluster looks just like a collection of independent individual isolated atoms.

Fortunately in our approach we can freely tune the width of the central Gaussian (parameter ξ), thus continuously interpolating between two limiting cases. In the first case (studied in the previous section) of small values of ξ the core electrons are perfectly modeled whereas the outer shell is not. In the opposite case of large ξ, the quality of outer-shell modeling significantly increases at the cost of poorer modeling of the core electrons, which, however, do not play any role in the energy absorption in the considered regime.

Therefore we decided to try the case where half of the atom electrons are frozen (nine in our case) and the remaining half are free to move around. It looks reasonable as in the experiment each atom loses two electrons on average. Notice please that in a recent theoretical paper dealing with xenon [20] only the ionized electrons were allowed to move and the rest were attached to the nucleus, forming an effective Yukawa scattering potential.

This weak absorption should be contrasted with the behavior presented in Fig. 8. In this figure we plot the total absorbed energy measured in photons per atom as a function of time. The calculations are done for $\xi=0.5$ and two different cluster sizes of $N=55$ (the ground state of this cluster is depicted in Fig. 2) and $N=147$ atoms. The absorbed energy increases with the size of the cluster and reaches the experimental result of 20 photons per atom already for a 147-atom cluster. The decrease in the energy absorption speed after the maximum of the pulse visible for the 55-atom case corresponds to the destruction of collective electron oscillations by the cluster explosion.

Let us mention that the energy oscillations seen in Fig. 8 for the case of 147 atoms are of purely numerical origin. The tree-based multipole method [64–67] of calculating the Coulomb force has to deal with multiple scales of the system. It

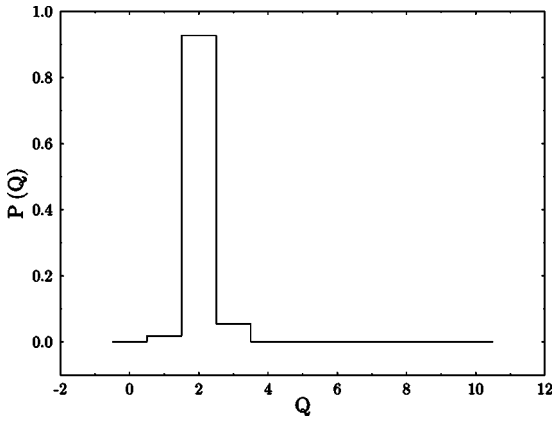

FIG. 9. Distribution of the final charges of the ions formed in the explosion of a 55-atom cluster.

has to properly model both the individual ions and the cluster as a whole. When the size of the system becomes sufficiently large energy oscillations appear. We have checked that they persist also for a smaller time step. Note, however, that these oscillations are small with respect to the absolute value of the cluster energy (cf. Fig. 3).

In Fig. 9 we plot the resulting distribution of the final charges of the ions formed in the explosion of the 55-atom cluster from Fig. 2 illuminated by a short-wavelength pulse. The result for the average ionization degree of two electrons per atom matches well the experimental result [19].

In Fig. 10 we present the structure of the cluster just after the pulse is finished. It shows that the atoms from the outer shells started to move. Still the atoms of the cluster stay together—the pulse itself was not able to totally disintegrate

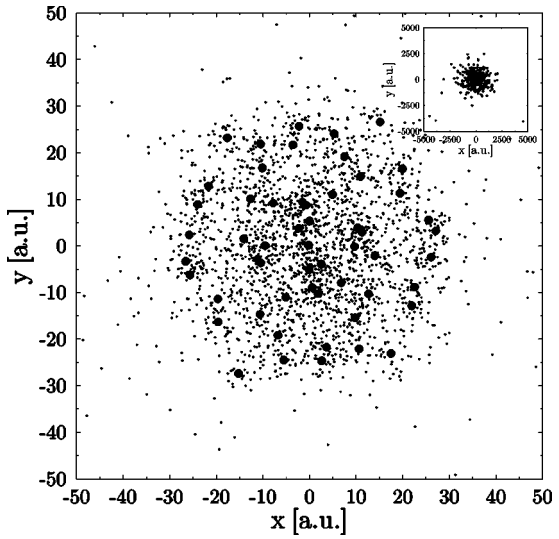

FIG. 10. Excited $N=55$-atom cluster from Fig. 2 at the end of the free-electron laser pulse at $t=100$ fs. Positions of the nuclei $\{\vec{R}_a\}$ are marked by filled circles. Small black dots correspond to the positions of the pseudoparticles modeling the electronic density ρ. An inset shows the electron cloud at a 1:100 magnification (i.e., the x and y coordinates vary from -5000 to 5000 a.u.). The size of the cluster is only about two times larger than the ground-state structure from Fig. 2.

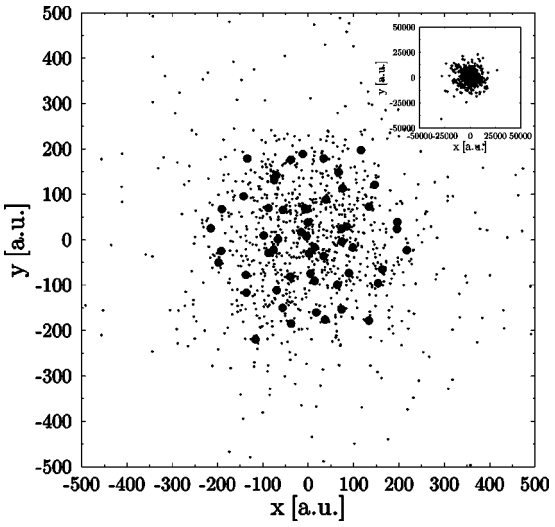

FIG. 11. Excited $N=55$-atom cluster with $\xi=0.5$ at $t=700$ fs. The inset shows the electron cloud at a 1:100 magnification (i.e., the x and y coordinates vary from $-50\,000$ to 50 000 a.u.).

the cluster, which is the case for optical frequencies. Although the electron cloud excited by the pulse is still well within the spatial structure of the cluster it already starts to affect the atoms forming the inner shells of the cluster. This could lead in principle to collisional ionization.

Another possible ionization mechanism is field ionization by the strong Coulomb field of the ions inside the cluster. Indeed, the inset to Fig. 10 shows the electron cloud at a 1:100 magnification. Most of the electrons remain still bound by the cluster as a whole but the size of this bound electron cloud is much larger than the size of the cluster. Thus the cluster core becomes positively charged, which leads to production of highly charged ions at the cluster surface. That it is indeed the case will be seen in the forthcoming figures.

In Fig. 11 we see the cluster structure after a longer time, namely, seven times as long as in the previous case. The cluster behavior is thus influenced by the period of "without-the-pulse" evolution. The outer shell is apparently moving away from the cluster but the atoms from the more deeply located shells are still close to each other. They continue, however, to be ionized by the excited electrons. The inset to Fig. 10 illustrates the isotropic character of the explosion (remember that the electric field of the laser pulse was polarized along the x axis).

As seen from Fig. 11 the cluster size is comparable with the optical case depicted in Fig. 4. There are still some electrons inside the cluster structure but the energies and charges of the ions hardly change if we further propagate the cluster in time. Thus in Fig. 12 we have the kinetic energy of the ions plotted as a function of the charge state. Both charges and energies were calculated at $t=700$ fs. As opposed to the optical case from Fig. 6 now the ions with higher charges come from the outer shells of the cluster. As already mentioned, one possible explanation of this result is the influence of the Coulomb field of the cluster core. It lowers the ionization potential for the ions from the outer shells of the cluster, facilitating their ionization.

Let us mention that a straight line seems to be a good approximation for the functional dependence in Fig. 12. This

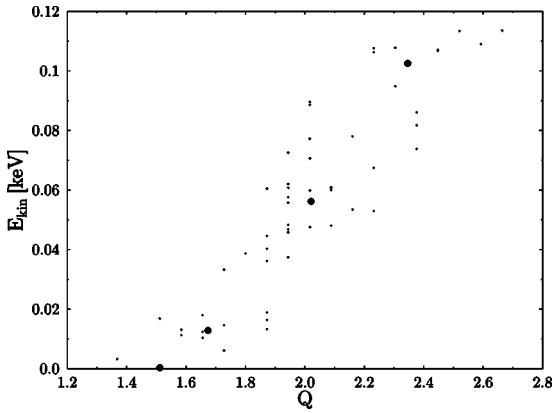

FIG. 12. Kinetic energy of the ions plotted as a function of the charge state in the short-wavelength case. Small dots correspond to individual ions while larger filled circles represent results averaged over (sub)shells.

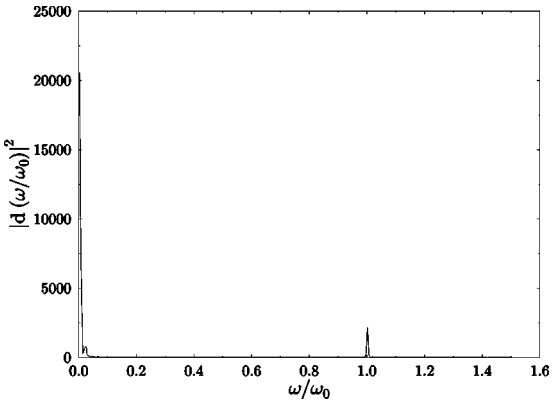

FIG. 13. Radiation spectrum of the cluster plotted as a function of the frequency relative to the frequency of the short-wavelength laser pulse.

could indicate a hydrodynamic explosion scenario [1,7] for the short-wavelength pulse.

To investigate the radiation spectrum of the cluster in the vacuum ultraviolet frequency regime, in Fig. 13 we have ploted the squared Fourier transform of the dipole moment d of the cluster as a function of time. There is a small peak corresponding to the original laser frequency out of the major part of the spectrum. Here, in contrast to the similar plot from Fig. 7 dealing with the optical case, no harmonics are visible. Thus the possible radiation occurs at much lower frequencies than the original laser frequency.

This can be understood by considering the ponderomotive energy of the electrons. It is given by the relation $E_p \propto I/\omega^2$ (I is the laser intensity and ω denotes its frequency) and in the case of the optical pulse used to produce the spectrum from Fig. 7 it is about 500 times larger that in the case of the short-wavelength pulse corresponding to Fig. 13. Thus the electrons illuminated by the short-wavelength pulse react much more sluggishly to the driving laser field and just do not want to move with its frequency.

VI. BRIEF SUMMARY

Using a rather simplified yet powerful approach we have addressed a "hot" topic in the field of cluster physics, namely, that of rare-gas atomic cluster explosion driven by a short x-ray pulse absorption. Despite its simplicity our time-dependent Thomas-Fermi model happened to provide a quite realistic description of both the ionization and explosion processes. Using the pulse parameters of the actual experiments we have obtained quite impressive qualitative agreement with the measured quantities.

Let us stress that our simple unified model encompasses two different cases and, surprisingly enough, enables us to track down two different physical mechanisms responsible for the explosion dynamics in both considered regimes. It seems that in the realm of optical frequencies the electrons are released mainly by the external laser field (above-the-barrier ionization process). The static electric fields of the other ions play only a minor role in lowering the ionization barrier. The released electrons are driven to move back and forth along the polarization axis of the laser wave. We suspect that they cause inner-shell atoms to be more ionized than those from the outer shell. The physical reason for that could be the fact that due to Coulomb expansion of the ions, the inner-shell atoms are more likely to be hit by the moving electrons.

In the ultraviolet regime, the physical mechanism seems to be different. First of all, the pulses do not directly ionize the atoms but rather excite the electrons. As a result the electron cloud expands isotropically, still being bounded by the cluster as a whole. As a natural consequence, the inner part of the cluster becomes positively charged and the resulting Coulomb field lowers the ionization barrier, facilitating ionization of atoms, especially of the outer shells.

It also seems that our model is able to reproduce the strong energy absorption observed in the experiment and, beyond that, provides a framework for explaining and interpreting this phenomenon. Moreover, the nonlinearity inherent in our model allows us to look further toward even stronger-intensity regimes. This line of development will be pursued in a forthcoming paper.

ACKNOWLEDGMENT

This work was supported by the Polish Committee for Scientific Research (KBN) under Grant No. 5 P03B 063 20.

[1] T. Ditmire, T. Donnelly, A. M. Rubenchik, R. W. Falcone, and M. D. Perry, Phys. Rev. A **53**, 3379 (1996).
[2] A. McPherson, B. D. Thompson, A. B. Borisov, K. Boyer, and C. K. Rhodes, Nature (London) **370**, 631 (1994).
[3] A. McPherson, T. S. Luk, B. D. Thompson, A. B. Borisov, O. B. Shiryaev, X. Chen, K. Boyer, and C. K. Rhodes, Phys. Rev. Lett. **72**, 1810 (1994).
[4] T. Ditmire, T. Donnelly, R. W. Falcone, and M. D. Perry, Phys. Rev. Lett. **75**, 3122 (1995).
[5] E. M. Snyder, S. A. Buzza, and A. W. Castleman, Jr., Phys. Rev. Lett. **77**, 3347 (1996).
[6] M. Lezius, S. Dobosz, D. Normand, and M. Schmidt, J. Phys. B **30**, L251 (1997).
[7] T. Ditmire, J. W. G. Tisch, E. Springate, M. B. Mason, N. Hay, R. A. Smith, J. Marangos, and M. H. R. Hutchinson, Nature (London) **386**, 54 (1997).
[8] M. Lezius, S. Dobosz, D. Normand, and M. Schmidt, Phys. Rev. Lett. **80**, 261 (1998).
[9] Y. L. Shao, T. Ditmire, J. W. G. Tisch, E. Springate, J. P. Marangos, and M. H. R. Hutchinson, Phys. Rev. Lett. **77**, 3343 (1996).
[10] T. Ditmire, J. W. G. Tisch, E. Springate, M. B. Mason, N. Hay, J. P. Marangos, and M. H. R. Hutchinson, Phys. Rev. Lett. **78**, 2732 (1997).
[11] T. Ditmire, Phys. Rev. A **57**, R4094 (1998).
[12] K. Ishikawa and T. Blenski, Phys. Rev. A **62**, 063204 (2000).
[13] I. Last and J. Jortner, Phys. Rev. A **62**, 013201 (2000).
[14] I. Last and J. Jortner, Phys. Rev. Lett. **87**, 033401 (2001).
[15] C. Siedschlag and J. M. Rost, Phys. Rev. Lett. **89**, 173401 (2002).
[16] C. Rose-Petruck, K. J. Schafer, K. R. Wilson, and C. P. J. Barty, Phys. Rev. A **55**, 1182 (1997).
[17] V. Véniard, R. Taïeb, and A. Maquet, Phys. Rev. A **65**, 013202 (2001).
[18] H. Wabnitz *et al.*, Nature (London) **420**, 482 (2002).
[19] T. Laarmann, A. R. B. de Castro, P. Gürtler, W. Laasch, J. Schulz, H. Wabnitz, and T. Möller, Phys. Rev. Lett. **92**, 143401 (2004).
[20] R. Santra and C. H. Greene, Phys. Rev. Lett. **91**, 233401 (2003).
[21] M. Rusek, H. Lagadec, and T. Blenski, Phys. Rev. A **63**, 013203 (2001).
[22] M. Brewczyk, C. W. Clark, M. Lewenstein, and K. Rzążewski, Phys. Rev. Lett. **80**, 1857 (1998).
[23] M. Brewczyk and K. Rzążewski, Phys. Rev. A **60**, 2285 (1999).
[24] M. Rusek and A. Orłowski, Acta Phys. Pol. A **105**, 425 (2004).
[25] M. Rusek and A. Orłowski, Acta Phys. Pol. A **106**, 3 (2004).
[26] L. Hernquist, Astrophys. J. **404**, 717 (1993).
[27] L. B. Lucy, Astron. J. **82**, 1013 (1977).
[28] R. Gingold and J. Monaghan, Mon. Not. R. Astron. Soc. **181**, 375 (1977).
[29] D. Wood, Mon. Not. R. Astron. Soc. **194**, 201 (1981).
[30] R. Gingold and J. Monaghan, Mon. Not. R. Astron. Soc. **197**, 461 (1981).
[31] R. Gingold and J. Monaghan, Mon. Not. R. Astron. Soc. **204**, 715 (1983).
[32] J. Monaghan and J. Lattanzio, Astron. Astrophys. **158**, 207 (1985).
[33] G. Phillips and J. Monaghan, Mon. Not. R. Astron. Soc. **216**, 883 (1985).
[34] M. Nagasawa and S. Miyama, Prog. Theor. Phys. **78**, 1250 (1987).
[35] T. Theuns, Ph.D. thesis, Vrije Universiteit, Brussels 1991.
[36] L. Brookshaw, Ph.D. thesis, Monash University 1986.
[37] H. Pongracic, S. Chapman, J. Davies, M. Disney, A. Nelson, and A. Whitworth, Mon. Not. R. Astron. Soc. **256**, 291 (1993).
[38] S. J. Chapman, Ph.D. thesis, University of Wales, 1992.
[39] J. Goodman and L. Hernquist, Astron. J. **378**, 637 (1991).
[40] J. Davies, Ph.D. thesis, University of Wales, 1991.
[41] L. H. Thomas, Proc. Cambridge Philos. Soc. **23**, 542 (1926).
[42] E. Fermi, Z. Phys. **48**, 73 (1928).
[43] P. Hohenberg and W. Kohn, Phys. Rev. **136**, B864 (1964).
[44] W. Kohn and L. J. Sham, Phys. Rev. **140**, A1133 (1965).
[45] L. A. Wittwer and S. D. Bloom, Phys. Rev. A **8**, 2249 (1973).
[46] S. M. Susskind, E. J. Valeo, C. R. Oberman, and I. B. Bernstein, Phys. Rev. A **43**, 2569 (1991).
[47] W. Benz, in *The Numerical Modeling of Nonlinear Stellar Pulsations*, edited by J. R. Buchler (Kluwer, Dordrecht, 1990), pp. 269–288.
[48] J. J. Monaghan, Annu. Rev. Astron. Astrophys. **30**, 543 (1992).
[49] F. Bloch, Z. Phys. **81**, 363 (1933).
[50] J. A. Ball, J. A. Wheeler, and E. L. Fireman, Rev. Mod. Phys. **45**, 333 (1973).
[51] K. Ishikawa, B. U. Felderhof, T. Blenski, and B. Cichocki, J. Plasma Phys. **60**, 787 (1998).
[52] M. Brewczyk, K. Rzążewski, and C. W. Clark, Phys. Rev. A **52**, 1468 (1995).
[53] N. H. March, in *Theory of the Inhomogeneous Electron Gas*, edited by S. Lundqvist and N. March (Plenum Press, New York, 1983), pp. 1–77.
[54] P. Gombas, *Die Statistische Theorie des Atoms und ihre Anwendungen* (Springer, Vienna, 1949).
[55] J. Farges, M. F. de Faraudy, B. Raoult, and G. Torchet, J. Chem. Phys. **78**, 5067 (1983).
[56] J. Farges, M. F. de Faraudy, B. Raoult, and G. Torchet, J. Chem. Phys. **84**, 3491 (1986).
[57] J. A. Northby, J. Chem. Phys. **87**, 6166 (1987).
[58] D. Wales and J. Doye, J. Phys. Chem. A **101**, 5111 (1997).
[59] http://www-wales.ch.cam.ac.uk/~jon/structures/LJ.html
[60] E. D. Potter, Q. Liu, and A. H. Zewail, Chem. Phys. Lett. **200**, 605 (1992).
[61] E. Teller, Rev. Mod. Phys. **34**, 627 (1962).
[62] J. Purnell, E. M. Snyder, S. Wei, and A. W. Castelman, Chem. Phys. Lett. **229**, 333 (1994).
[63] M. Brewczyk and K. Rzążewski, J. Phys. B **34**, L289 (2001).
[64] A. W. Appel, SIAM (Soc. Ind. Appl. Math.) J. Sci. Stat. Comput. **6**, 85 (1985).
[65] J. E. Barnes and P. Hut, Nature (London) **324**, 446 (1986).
[66] L. Greengard, Comput. Phys. **4**, 142 (1990).
[67] L. Greengard, Science **265**, 909 (1994).